Supplementary Information

Supplementary Results

Binding experiments with H4 peptides. We analyzed the interaction between ADD_{3A} and N-terminally acetylated histone H4 peptide (residues 1-20) with and without symmetrical dimethylation on H4R3 (H4R3me0; H4R3me2s) using ITC and NMR. Zhao and co-workers demonstrated an interaction between ADD_{3A} and N-terminally acetylated residues 1-20 of H4 using a pull-down experiment (Zhao *et al*, 2009). Although a small amount of heat emission was detected when ADD_{3A} was added to the H4R3me0 peptide solution in a buffer containing 25 mM HEPES-NaOH, 100 mM NaCl and 0.1 mM TCEP at pH 7.4, the heat emitted was so small that we could not determine the binding affinity (data not shown). For the H4R3me2s peptide, no significant heat was detected when ADD_{3A} was added (data not shown). We also analyzed the interaction of ADD_{3A} with the H4R3me0 and H4R3me2s peptides using NMR titration experiments in a buffer containing 10 mM Tris-HCl, 50 mM NaCl and 2 mM DTT at pH 7.0. In contrast to the titration of the H3 peptide, which showed slow exchange (supplementary Fig. S5A), several cross peaks exhibited chemical shift changes in the fast exchange regime on the NMR time scale, suggesting that both of the H4 peptides bind to ADD_{3A} more weakly than does the H3 peptide (supplementary Fig. S8). The K_D values of the H4R3me0 and H4R3me2s peptides were estimated to be 150 μM and 250 μM, respectively, by monitoring the chemical shifts of the main chain amide group of Gly543. In addition, we measured the NMR spectrum of ^{15}N-labeled ADD_{3A} in the presence of 4 equimolar H4R3me0 or H4R3me2s peptide. The measurements were made under buffer conditions containing 420 mM NaCl, similar to those in the pull-down binding experiment of Zhao *et al.* The spectra were very similar to the spectrum recorded without H4 peptide in buffer containing 420 mM NaCl (data not shown). Taken together, our ITC and NMR experiments suggest that both the H4R3me0 and H4R3me2s peptides bind much more weakly to ADD_{3A} than the H3 peptide does. Zhao *et al.* used N-terminally acetylated H3 and H4 tails in their pull-down experiments. Our data suggest that N-terminal acetylation of the H3 tail largely impedes binding to ADD_{3A} (Table 1).

Interaction surface of ADD_{3A} with the H3-tail in unlinked complex. To examine whether the mode of interaction between ADD_{3A} and the H3-tail in the fusion protein is the same as that of the non-fused ADD_{3A}:H3-tail complex, we performed a chemical shift perturbation experiment. ^{15}N-labeled ADD_{3A} was titrated with unlabeled $H3_{1-19}$ peptide, and chemical shift changes of the main chain amides of ADD_{3A} were observed in ^{1}H-^{15}N correlation spectra (supplementary Fig. S5A). Of 135 cross peaks whose assignments were obtained, 37 showed chemical shift changes

larger than 0.1 ppm in ^{1}H or 0.5 ppm in ^{15}N . These residues are largely confined to the groove of ADD_{3A}, in which the H3-tail fits in the crystal structure of the H3-tail: ADD_{3A} fusion protein. Thus, the resulting chemical shift perturbations are consistent with the crystal structure, suggesting that the interactions observed between ADD_{3A} and the H3-tail in the crystal are not artificially generated by the link between them (supplementary Fig. S5B). Almost identical chemical shift perturbations were observed in the NMR titration experiment with the 10mer H3 peptide, $H3_{1-10}$. During the titration of the H3-tail, all the shifted resonances of ADD_{3A} were in the slow exchange regime on the NMR time scale, which is consistent with the tight binding shown by the ITC experiments. Collectively, the structural features observed in the fusion complex are highly likely to reflect the interaction between ADD_{3A} and the H3-tail in solution.

Supplementary discussion

Comparison between H3 interfaces of ADD_{3A} and ADD_{3L}. The higher H3-binding affinity of ADD_{3A} may be attributable to the substitution of two residues, Ile576 and Met548, that are located at the histone interface of ADD_{3A} (supplementary Figs. S2A and S2B). One of these residues, Met548 of ADD_{3A}, is positioned at the center of the H3 binding cleft. This residue has a larger contact surface (96.18 $Å^2$) with the H3 peptide than the corresponding residue in the ADD_{3L}-H3 complex, i.e., Ile107 in the ADD_{3L}-H3 structure (59.73 $Å^2$, Ooi *et al*, 2007). The other residue, Ile576 of ADD_{3A}, forms a hydrophobic pocket with Leu547, Ala575 and Trp581, which makes hydrophobic contacts with the methyl groups of Ala1 and Thr3 of histone H3. In contrast, ADD_{3L} has His135 in place of Ile576 of ADD_{3A} and seems to pack less tightly against Thr3 of histone H3 (Ooi *et al*, 2007). These contacts may result in ADD_{3A} binding more strongly to the H3 tail than does ADD_{3L}.

In the present structure of the ADD_{3A}-H3 tail complex, Lys9 makes contacts with ADD_{3A}. However, no electron densities were observed for Arg8 and Lys9 of H3 in the ADD_{3L}-H3 tail complex (Ooi *et al,* 2007; supplementary Fig. S2D). We assume that the ADD_{3A} contacts that are formed by the side chain of Lys9 are not caused by the covalent link between the N-terminus of ADD_{3A} and the C-terminus of H3 peptide, because the ^{1}H and ^{15}N chemical shifts of the main chain amides of Cys541 and Tyr536 (with which Lys9 makes the contacts in the crystal structure) changed on binding to the H3 peptide in the NMR titration experiment (supplementary results; supplementary Fig. S5). However, the contribution of these contacts to the affinity between ADD_{3A} and the H3 tail seem to be relatively small because substitution of Lys9 with cysteine or methylated lysine analogues resulted in no significant change in the affinity (Table 1).

Recognition of H3R2. Several PHD fingers that bind to H3K4me3, such as the fingers of BPTF and ING2, have acidic residues that interact electrostatically with unmodified H3R2 on the H3 binding surface. (Li *et al*, 2006; Peña *et al*, 2006; supplementary Fig. S4D). The methylation of H3R2 has been reported to inhibit the interactions of these fingers with H3 (Iberg *et al*, 2008). However, the ADD_{3A}-H3 interaction is independent of the methylation status of H3R2. ADD_{3A} lacks acidic residues at the corresponding binding site for H3R2 and instead possesses a tyrosine residue, Tyr533 (supplementary Fig. S4A). This structural feature is conserved in the ADD domains of DNMT3A and DNMT3L (supplementary Fig. S4B), and is similar to the PHD finger of RAG2, which recognizes methylated H3R2 through a π-π stacking interaction with its Tyr445 (Ramón-Maiques *et al*, 2007; supplementary Fig. S4C).

Supplementary Methods

Protein Expression and Purification. A DNA fragment encoding ADD_{3A} was amplified by PCR and cloned into a bacterial expression vector pGEX6P-1 (GE Healthcare Biosciences) containing a N-terminal Glutathione-S-transferase (GST) tag. ADD_{3A} was overexpressed in *E. coli* strain BL21(DE3). Cells were grown at 37 °C in Luria–Bertani medium (LB) containing 50 μg/ml ampicillin and 20 μM zinc acetate to an optical density of 0.5–0.6 at 660 nm, and then induced with 0.2 mM isopropyl β-d-thiogalactoside (IPTG) for 15 hours at 18 °C. For preparation of ^{15}N-labeled or $^{15}N,^{13}C$- double labeled ADD_{3A}, M9 minimal media containing 0.5 g/L $^{15}NH_4Cl$ or 0.5 g/L $^{15}NH_4Cl$ and 1 g/L ^{13}C glucose was used instead of LB media. The following steps were carried out at 4°C. Cells were harvested by centrifugation, and lysed by sonication in 50 mM Tris-HCl pH 8.0 buffer containing 300 mM NaCl, 1 mM dithiothreitol (DTT), 5% glycerol, 0.1% Triton X-100, 1 mM phenylmethylsulfonyl fluoride (PMSF) and 20 μM zinc acetate. The clarified lysate was loaded onto Glutathione Sepharose 4 Fast Flow beads (GE Healthcare) after the debris was removed by centrifugation. ADD_{3A} was eluted from the beads by releasing from the GST tag with PreScission protease (GE Healthcare Biosciences). Subsequently, the eluted protein was concentrated and loaded onto a HiLoad 16/60 Superdex 75 (GE Healthcare Biosciences) column equilibrated with 10 mM Tris–HCl buffer pH 8.0 containing 150 mM NaCl and 2 mM DTT. Purified protein was concentrated to 10 mg ml^{-1} using an Amicon Ultra 3,000 cut-off membrane concentrator (Millipore).

The DNA fragment encoding an N-terminal fragment of histone H3 (amino-acid residues 1-20) fused with ADD_{3A} (amino-acid residues 476-614) was cloned into a pGEX4T-3 vector (GE Healthcare Bio-Sciences) engineered for protein expression with an N-terminal GST and small ubiquitin-like modifier-1 (SUMO-1) fusion tag, generating a construct with no additional residues at the N-terminus of the histone H3-tail after removal of the tag by SUMO specific protease SENP2. The H3-tail:ADD_{3A} fusion protein was overexpressed in *E. coli* strain

BL21(DE3) and purified by GST affinity column chromatography. The GST-SUMO tag was cleaved off with SENP2 on the glutathione beads, resulting in elution of the H3-tail:ADD_{3A} fusion protein. The eluted protein was further purified in the same manner as ADD_{3A}. The $CD_{HP1\alpha}$ (residues 15-78) was bacterially expressed as a GST-SUMO1-fusion protein. GST-SUMO1-$CD_{HP1\alpha}$ was digested by SENP2. GST fused $CD_{HP1\alpha}$ was prepared for GST pull-down assays. For preparation of isotope-labeled protein samples, M9 minimal media was used instead of LB media. The ADD of DNMT3L (residues 35-174) was expressed as a GST-SUMO1 fusion protein, and was purified in the same manner as ADD_{3A}.

H3 peptide preparation and *in vitro* binding assay. An N-terminal peptide derived from histone H3 (residues 1-19) with an additional tryptophan residue at its C-terminus, which allowed us to determine the peptide concentration by measuring absorbance at 280 nm, was cloned into a modified pGEX4T-3 vector. The H3 peptide was expressed in BL21(DE3) for 3 hours at 37 °C induced by 0.5 mM IPTG. After cell lysis and GST affinity purification, the GST-SUMO tag was removed by digestion with SENP protease and the peptide was purified using acetone precipitation and reversed phase HPLC on a C18 column with an acetonitrile gradient in the presence of 0.05% trifluoroacetic acid.

H3 peptide analogues harboring non-, di- or trimethylated lysine were prepared by alkylation of cysteine residues as described previously (Simon *et al*, 2007).We treated 100 μM peptide carrying the K4C or K9C mutation with 10 mM DTT for 1 hour, followed by alkylation of the cysteine using distinct conditions for each methylation variant. To prepare the non-methylated lysine analogue, we treated the peptide with 200 mM (2-chloroethyl) ammonium chloride in 1M Tris-HCl (pH=8.5) at 37 °C for 4 hours. The reaction was then stopped by adding 0.7 M β-mercaptoethanol. The yield of the reaction was 80~90%. For the di- and trimethylated lysine analogues, we used the same conditions as those reported by Simon *et al.*, and the yield was almost 100%. The product peptides were then separated from the unreacted peptides using reverse-phase HPLC and used in the ITC experiments. All peptide samples were analyzed by mass spectrometry performed on an ABI Voyager Elite MALDI-TOF (Applied Biosystems).

The structure of the ADD_{3A}-H3 tail complex shows that most parts of the side chain of H3K4 make contacts with ADD_{3A}, through hydrophilic contacts at the terminal amino group and through hydrophobic contacts at the alkyl chain moiety. Therefore, it might be possible that the approximately two-fold smaller binding affinity of the H3 peptide harboring the cysteine-derived lysine analogue to ADD_{3A} (Table 1) is at least partly due to the weaker packing of the lysine analogue caused by the sulfur atom at the β position.

We purchased the following histone peptides from Toray Research Center (Tokyo, Japan) which are chemically synthesized: $H3_{1-10}$, $H3R2me2a_{1-15}$, $Ac\text{-}H3_{1-19}$, $Ac\text{-}H4_{1-20}$ and

Ac-H4R3me2s$_{1-20}$.

Isothermal titration calorimetry (ITC) measurements were performed in 25 mM HEPES-NaOH buffer (pH 7.4) containing 100 mM NaCl and 0.1 mM TCEP on a MicroCal VP-ITC instrument at 25 °C. Protein solutions were exchanged into the ITC measurement buffer by gel-filtration chromatography or dialysis. Lyophilized histone H3 peptides were dissolved in the same buffer. The peptide solution at 10-20 μM in the calorimetric cell was titrated with protein solution at 200-600 μM. Binding constants were calculated by fitting the data using the ITC data analysis module of Origin 7.0 (OriginLab Corporation).

Data collection and structure determination. X-ray diffraction data sets were processed with the program HKL2000 (Otwinowski, 1997). The structure of unliganded $ADD_{3A}$was solved by the multiwavelength anomalous dispersion method using the programs SOLVE and RESOLVE (Terwilliger, 2000; Terwilliger & Berendzen, 1999). The model was built using the program COOT (Emsley & Cowtan, 2004) and refined against the data collected at a wavelength of 1.0 Å using REFMAC (Murshudov *et al*, 1997) from the CCP4 suite, yielding a crystallographic R factor of 20.9% and a free R factor of 25.0% to 2.3 Å. The structure of the H3-tail:ADD_{3A} fusion protein was solved by a molecular replacement method with the program Molrep from the CCP4 suite (Vagin & Teplyakov, 1997), using the free-form structure of ADD_{3A} as a search model and refined against data to 2.3 Å resolution with a crystallographic R factor of 19.2% and free R factor of 22.0%. The final model contains residues 1-9 and 17-20 of the H3 tail, residues 476-610 of ADD_{3A}, 37 water molecules and seven ethyleneglycol molecules. The H3 residues 17-20 folded as an extension of the N-terminal α-helix of ADD_{3A}. Considering the crystal packing and connectivity in the poor electron density for the H3 residues 10-16, it is inferred that ADD_{3A} interacts with the H3 peptide within the same polypeptide chain in the crystal of the fusion protein. The diffraction and refinement data are summarized in supplementary Tables 1 and 2. The stereochemical quality of the final models was assessed using PROCHECK (Laskowski *et al*, 1993). All figures of protein molecules were produced using PyMOL (W. L. DeLano; http://www.pymol.org). Buried surface area analysis was carried out using the PISA server (Krissinel & Henrick, 2007).

NMR spectroscopy. Backbone resonances of ADD_{3A} in the unliganded state were assigned by using 3D HNCO, HN(CA)CO, HNCA, HN(CO)CA, HNCACB, and CBCA(CO)NH. Peptide titration experiments were performed by stepwise addition of concentrated H3 peptide stock solutions into 400-μl samples of 100 μM ^{15}N-labeled ADD_{3A}. The NMR competition assay was performed as described previously (Suzuki *et al*, 2008). ^{15}N-labeled ADD_{3A} at the concentration of 90-100 μM was first titrated by unlabeled K9me2-H3 or K9me3-H3 peptide at 110-120 μM

and then titrated by unlabeled 1.8-2.2 mM $CD_{HP1\alpha}$. Reciprocally, ^{15}N-labeled $CD_{HP1\alpha}$ at 100 μM was first titrated by unlabeled H3K9me3 peptide to 1.25 molar equiv and then titrated by unlabeled 510 μM ADD_{3A}. The K_D values of the interactions between $CD_{HP1\alpha}$ and K9me2-H3 or K9me3-H3 peptide were calculated from the peak height ratio of H3-bound to the free-form ^{15}N-ADD_{3A} in the spectra of the ^{15}N-labeled ADD_{3A} in the presence of H3K9me2 or H3K9me3 peptide and 10 or 21 molar equiv of $CD_{HP1\alpha}$. The assignments of ^{1}H-^{15}N cross peaks of backbone amides of ADD_{3A} in the H3-tail complex were obtained based on assumption of minimum chemical shift perturbation from those of unliganded protein.

GST pull-down assay GST pull-down assays were carried out with Glutathione sepharose 4FF (GE Healthcare) in the same buffer used in the ITC measurements. GST-fused $CD_{HP1\alpha}$ (residues 15-78) and GST-ADD_{3A}, each attached to the glutathione beads, were incubated with 25 μM H3K9me2 or H3K9me3 analog peptides in the presence of 0 to 250 μM ADD_{3A} and $CD_{HP1\alpha}$, respectively. The beads were extensively washed with the binding buffer containing 0.2% Triton X-100 and analyzed by 15% SDS polyacrylamide gel electrophoresis followed by CBB stain.

Supplementary Figure S1

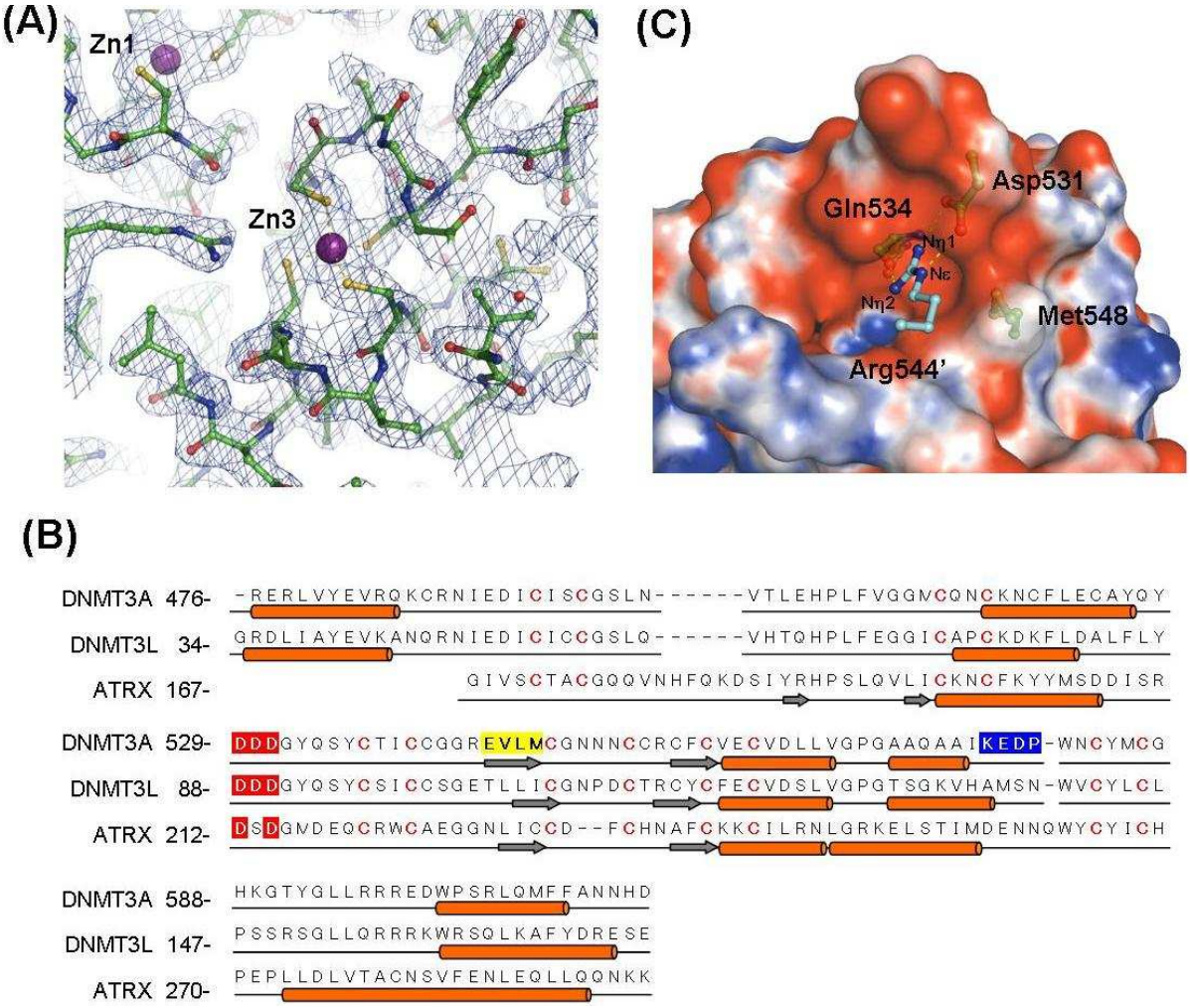

Fig. S1 | Structure of ligand-free ADD_{3A}. **(A)** Refined $2F_O$-F_C map contoured at 1.0 σ around Zn-3 coordinated by two CxxC motifs in the free-form structure of ADD_{3A}. **(B)** Multiple sequence alignment of ADD domains. Secondary structural elements of each ADD domain are indicated below the sequences. α-helices and β-strands are shown by orange cylinders and gray arrows, respectively. Acidic residues forming the H3K4 binding pockets are highlighted in red. Cysteine residues coordinating zinc ions are indicated in red. The H3N loop and β1 residues of ADD_{3A} are highlighted in blue and yellow, respectively. **(C)** Close-up view of the H3K4 binding pocket. The guanidino group of Arg544' from a symmetry-related molecule occupies the acidic pocket consisting of three aspartic acid residues, Asp529, Asp 530 and Asp 531. The side chain carbonyl group of Asp531 forms hydrogen bonds with the Nη1 and Nε atoms of Arg544'. The main chain carbonyl group of Gln534 forms hydrogen bonds with the Nη2 of Arg544'. The residues that form the H3K4 binding pocket has also been observed in ADD_{3L}

Supplementary Figure S2

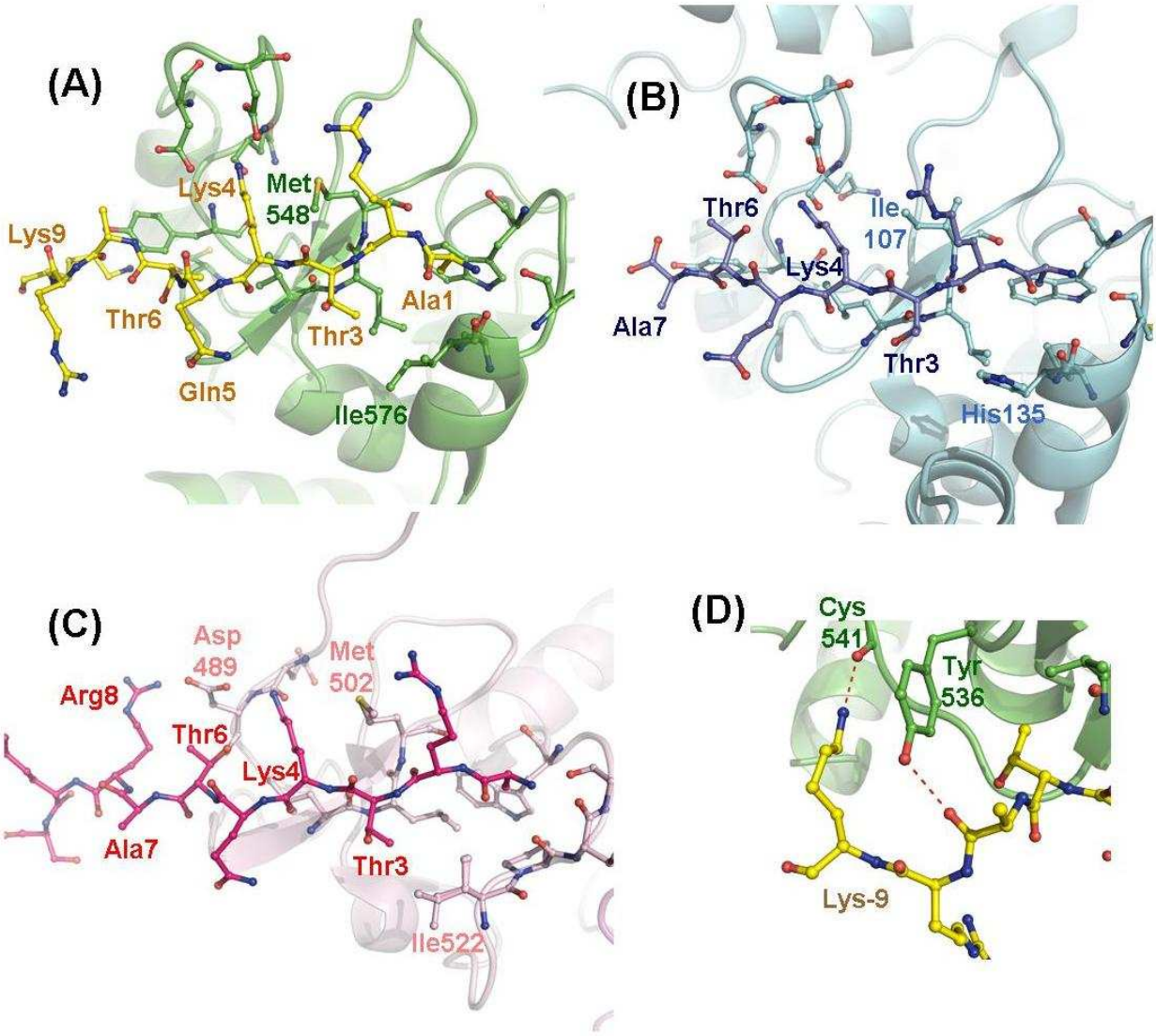

Fig. S2 | Structural comparison between the histone H3 tail bound to ADD_{3A} **(A)**, ADD_{3L} **(B)** and the PHD of BHC80 (PHD_{BHC80}) **(C)** (PDB code: 3A1B, 2PVC and 2PUY, respectively). The ribbon and stick representation of protein models of ADD_{3A}, ADD_{3L} and PHD_{BHC80} are shown in green, cyan and pink, respectively. The H3 tail peptide bound to these proteins are shown as stick models in yellow, blue and red, respectively. The regions from H3A1 to H3Q5 of the H3 peptide bound to ADD_{3A} adopts the similar conformation to those bound to ADD_{3L} and, PHD_{BHC80} which recognize non-methylated H3K4 (Lan *et al*, 2007; Ooi *et al*, 2007), while the conformation of H3 peptide from H3T6 to H3K9 observed in the ADD_{3A}-H3 complex is slightly deviated from that in the PHD_{BHC80} -H3 complex. **(D)** Close-up view of the Lys9 contact site in the ADD_{3A}-H3 complex structure.

Supplementary Figure S3

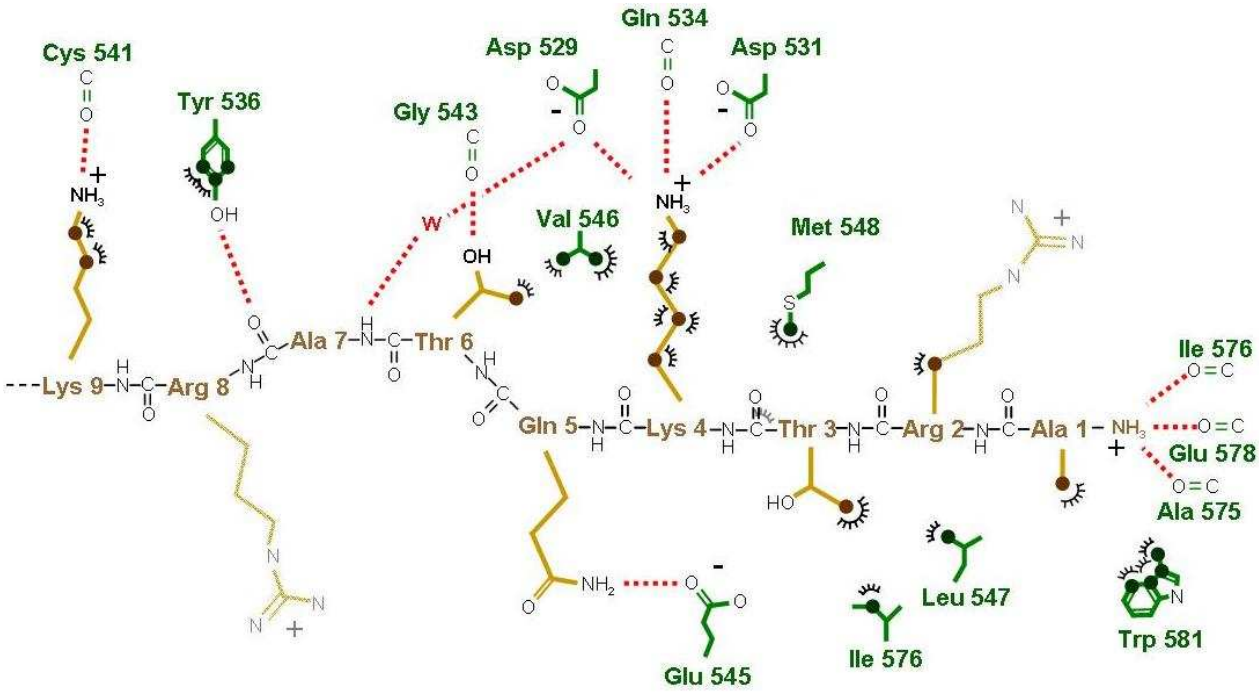

Fig. S3 | Schematic diagram of the ADD_{3A}:H3-tail interaction. Amino acid residues of ADD_{3A} involved in the H3-tail interaction are indicated. The main chain hydrogen bonds forming the inter-molecular β-sheet are not shown. Hydrogen bonds (<3.3 Å) between ADD_{3A} and the H3-tail are shown in red dotted lines, van der Waals contacts (<4.0 Å) are represented by semicircular arcs. 'W' represents a water molecule.

Supplementary Figure S4

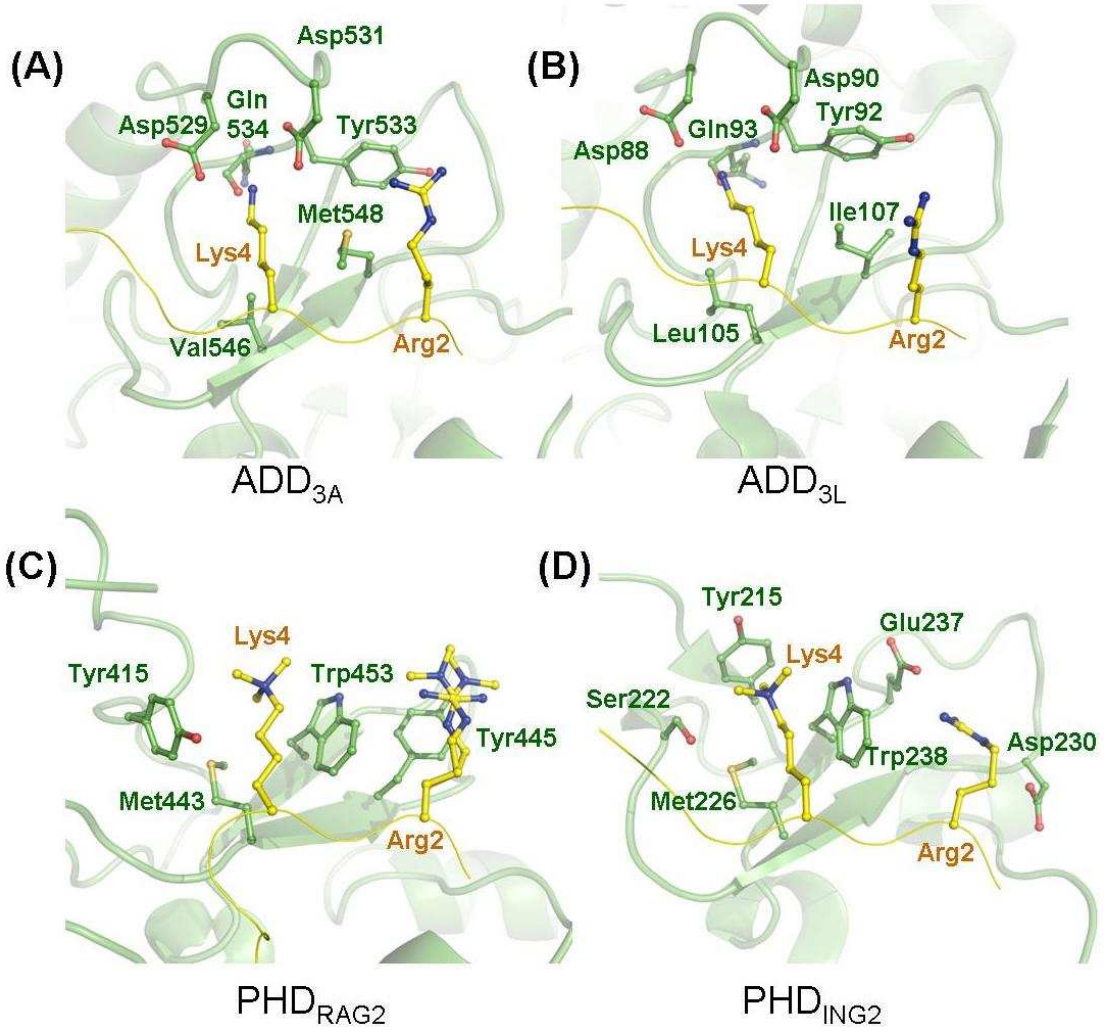

Fig. S4 | H3R2 binding pockets of PHD fingers. In the structure of ADD_{3A}-H3 complex **(A)**, the side chain of H3R2 is fully exposed to the solvent as is observed in the structure of DNMT3L-H3 complex (**B**, PDB code: 2PVC) and the methylation on this residue seems not to affect the interaction between ADD_{3A} and H3 tail. The PHD finger of RAG2 was reported to bind to the H3 tail carrying both methylated H3R2 and H3K4 with slightly higher affinity than to the tail carrying only methylated H3K4 (Ramón-Maiques *et al*, 2007). In the structure of PHD_{RAG2} complexed with methylated H3R2 (**C**, PDB code: 2V86), methylated side chain of H3R2 stacks with aromatic side chain of Tyr445. In contrast, it was proposed that the methylation of H3R2 generally impedes binding of effector proteins that recognize H3K4me3 (Iberg *et al*, 2008). In the PHD_{ING2}-H3 structure (**D**, PDB code: 2G6Q), the side chain of H3R2 makes electrostatic contacts with acidic residues of PHD_{ING2}. This type of H3R2 recognition is widely seen in the PHD finger-H3 complex structures and seems to be disrupted by methylation on H3R2.

Supplementary Figure S5

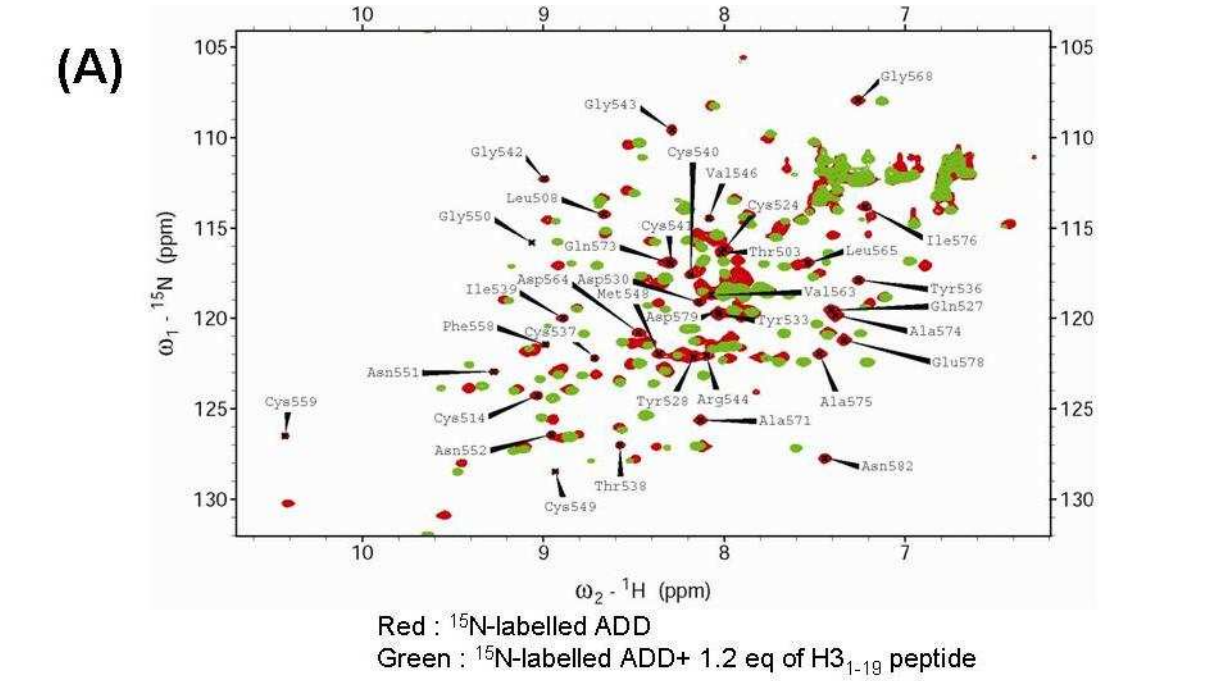

Fig. S5 | ^{1}H-^{15}N chemical shift perturbation upon H3 peptide binding. **(A)** ^{1}H-^{15}N HSQC spectra of free (red) and H3-bound ADD$_{3A}$ (green). Residues that undergo chemical shift changes larger than 0.1 ppm in ^{1}H or 0.5 ppm in ^{15}N upon H3 binding are indicated with labels. **(B)** Surface representation of ADD$_{3A}$. Surface residues that exhibited large chemical shifts upon binding, labeled in A, are highlighted in red. The H3 peptide bound to ADD$_{3A}$ in the fusion crystal is shown as stick model.

Supplementary Figure S6

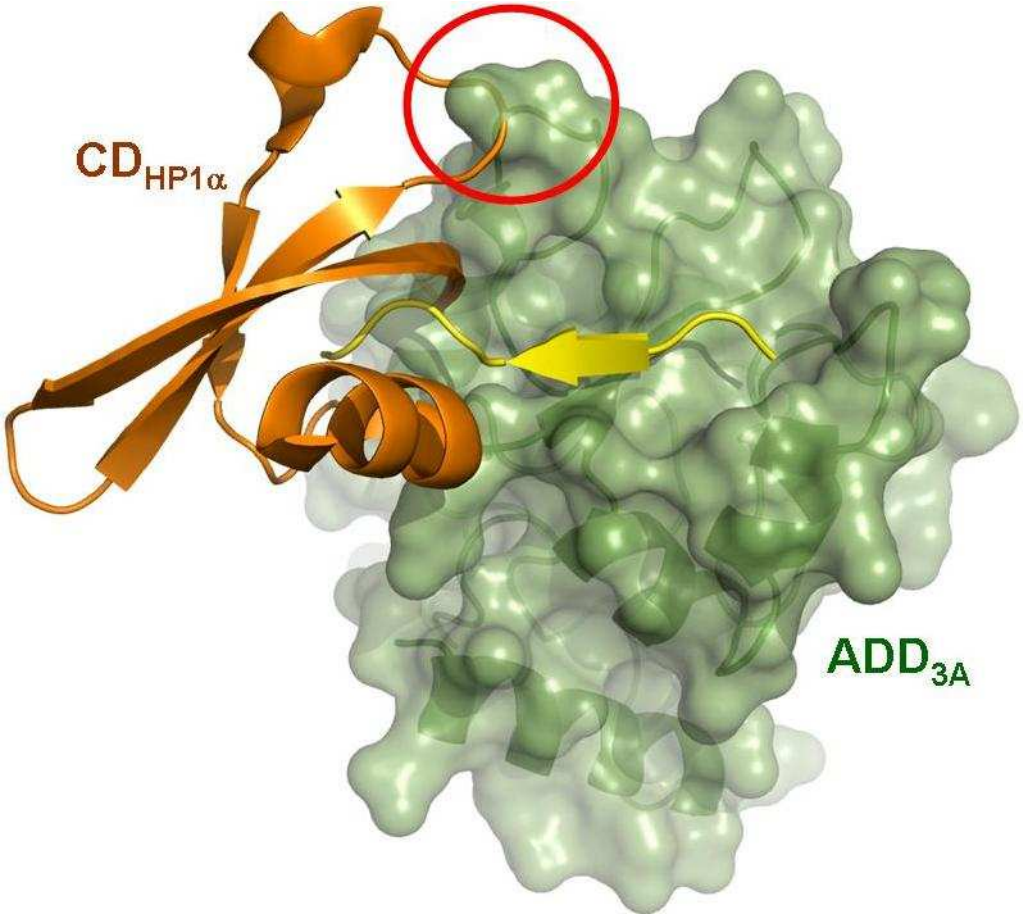

Fig. S6 | The model of the ternary complex of ADD_{3A} (green), $CD_{HP1\alpha}$ (orange) and H3-tail (yellow). The model was built by superimposing the Cα atoms of Gln5 and Thr6 of the H3 tail in the ADD_{3A}:H3-tail complex to the corresponding atoms in the $CD_{HP1\alpha}$: H3-tail complex (PDB entry; 3FDT). A red circle indicates the most significant structural collision between two proteins.

Supplementary Figure S7

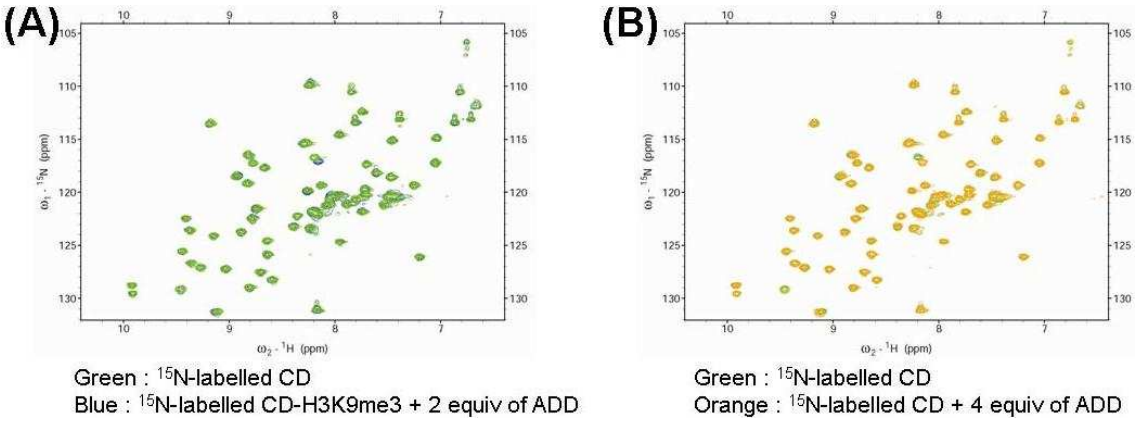

Fig. S7 | NMR binding experiments. **(A)** The spectrum of $CD_{HP1\alpha}$ (green) and $CD_{HP1\alpha}$ in the presence of 1.25-molar equiv of K9me3-H3 and 2-molar equiv of ADD_{3A} (blue). Dissociation of $CD_{HP1\alpha}$: K9me3H3-tail complex by ADD_{3A} was observed. **(B)** The spectrum of $CD_{HP1\alpha}$ (green) and $CD_{HP1\alpha}$ in the presence of 4-molar excess of ADD_{3A} (orange). No direct interaction between ADD_{3A} and $CD_{HP1\alpha}$ was observed.

Supplementary Figure S8

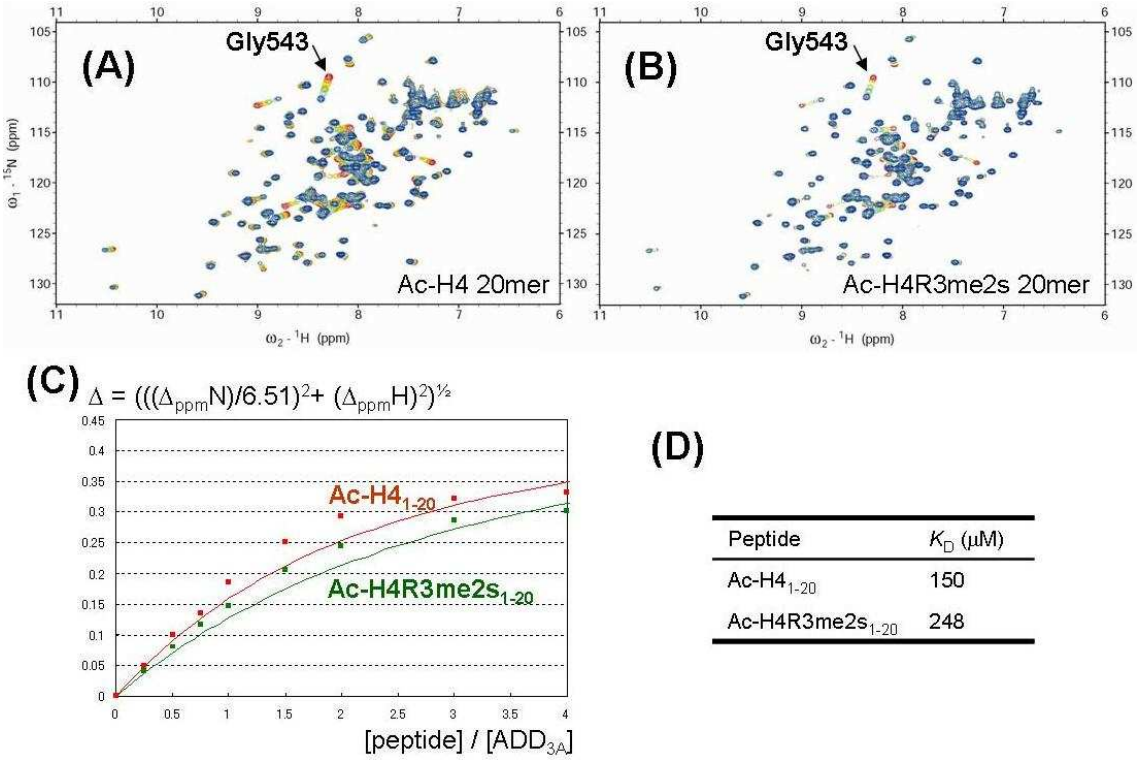

Peptide	K_D (μM)
Ac-H4$_{1-20}$	150
Ac-H4R3me2s$_{1-20}$	248

Fig. S8 | Binding experiment with N-terminus acetylated H4 tail without and with symmetrical dimethylation on Arg3 (Ac-H4 and Ac-H4R3me2s) using ^{1}H-^{15}N correlation spectra. ^{15}N-labeled ADD$_{3A}$ at the concentration of 100 μM was titrated by unlabeled Ac-H4 **(A)** or Ac-H4R3me2s peptide **(B)** from the peptide stock solutions at the concentration of 1.0 mM. The ^{1}H-^{15}N correlation spectra were recorded at the peptide to protein ratio of 0, 0.25, 0.5, 0.75, 1.0, 1.5, 2.0, 3.0 and 4.0 (red to blue). Almost identical peak shifts were observed regardless of the methylation status of H4R3. Nonlinear least-square fitting of the gradual peak shift of the backbone amide of Gly543 to the equation,

$$\Delta = \Delta_{\max} \times \left\{ \frac{([protein]_0 + [peptide]_0 + K_D) - \sqrt{([protein]_0 + [peptide]_0 + K_D)^2 - 4[protein]_0 \times [peptide]_0}}{2 \times [protein]_0} \right\}$$

where $\Delta = \sqrt{\left(\frac{\Delta_{ppm}N}{6.51}\right)^2 + (\Delta_{ppm}H)^2}$ was used to estimate K_D values of the interaction between ADD$_{3A}$ and H4 peptides (C,D).

References

Emsley P, Cowtan K (2004) Coot: model-building tools for molecular graphics. *Acta Crystallogr D Biol Crystallogr* **60:** 2126-2132

Iberg A, Espejo A, Cheng D, Kim D, Michaud-Levesque J, Richard S, Bedford M (2008) Arginine methylation of the histone H3 tail impedes effector binding. *J Biol Chem* **283:** 3006-3010

Krissinel E, Henrick K (2007) Inference of macromolecular assemblies from crystalline state. *J Mol Biol* **372:** 774-797

Lan F, Collins R, De Cegli R, Alpatov R, Horton J, Shi X, Gozani O, Cheng X, Shi Y (2007) Recognition of unmethylated histone H3 lysine 4 links BHC80 to LSD1-mediated gene repression. *Nature* **448:** 718-722

Laskowski R, Macarthur M, Moss D, Thornton J (1993) Procheck – a program to check the stereochemical quality of protein structures. *Journal of Applied Crystallography* **26:** 283-291

Li H, Ilin S, Wang W, Duncan E, Wysocka J, Allis C, Patel D (2006) Molecular basis for site-specific read-out of histone H3K4me3 by the BPTF PHD finger of NURF. *Nature* **442:** 91-95

Murshudov G, Vagin A, Dodson E (1997) Refinement of macromolecular structures by the maximum-likelihood method. *Acta Crystallogr D Biol Crystallogr* **53:** 240-255

Ooi S, Qiu C, Bernstein E, Li K, Jia D, Yang Z, Erdjument-Bromage H, Tempst P, Lin S, Allis C, Cheng X, Bestor T (2007) DNMT3L connects unmethylated lysine 4 of histone H3 to de novo methylation of DNA. *Nature* **448:** 714-717

Otwinowski ZaM, W. (1997) Processing of X-Ray Diffraction Data Collected in Oscillation Mode. In *Methods Enzymol.*, Sweet CWCJaRM (ed), Vol. 276, pp 307-326. New York: Academic Press

Peña P, Davrazou F, Shi X, Walter K, Verkhusha V, Gozani O, Zhao R, Kutateladze T (2006) Molecular mechanism of histone H3K4me3 recognition by plant homeodomain of ING2. *Nature* **442:** 100-103

Ramón-Maiques S, Kuo A, Carney D, Matthews A, Oettinger M, Gozani O, Yang W (2007) The plant homeodomain finger of RAG2 recognizes histone H3 methylated at both lysine-4 and arginine-2. *Proc Natl Acad Sci U S A* **104:** 18993-18998

Simon M, Chu F, Racki L, de la Cruz C, Burlingame A, Panning B, Narlikar G, Shokat K (2007) The site-specific installation of methyl-lysine analogs into recombinant histones. *Cell* **128:** 1003-1012

Suzuki C, Garces R, Edmonds K, Hiller S, Hyberts S, Marintchev A, Wagner G (2008) PDCD4 inhibits translation initiation by binding to eIF4A using both its MA3 domains. *Proc Natl Acad Sci U S A* **105:** 3274-3279

Terwilliger T (2000) Maximum-likelihood density modification. *Acta Crystallogr D Biol Crystallogr* **56:** 965-972

Terwilliger T, Berendzen J (1999) Automated MAD and MIR structure solution. *Acta Crystallogr D Biol Crystallogr* **55:** 849-861

Vagin A, Teplyakov A (1997) MOLREP: an Automated Program for Molecular Replacement. *Journal of Applied Crystallography* **30:** 1022-1025

Zhao Q, Rank G, Tan Y, Li H, Moritz R, Simpson R, Cerruti L, Curtis D, Patel D, Allis C, Cunningham J, Jane S (2009) PRMT5-mediated methylation of histone H4R3 recruits DNMT3A, coupling histone and DNA methylation in gene silencing. *Nat Struct Mol Biol*

Table S1 Crystallographic data and data collection statistics

Crystallographic data and Data collection statistics						
X-ray resource	PF BL-5					
Detector	ADSC Q315					
Crystal	ADD_{3A}					$H3\text{-}ADD_{3A}$
	Peak	Edge	High remote	Low remote		
Wave-length (Å)	1.28221	1.28333	1.25730	1.29001	1.00000	1.00000
Space group	$P6_122$	←	←	←	←	$P4_12_12$
Resolution (Å)[2]	50-(2.55)2.46	←	←	←	50-(2.38)2.3	50-(2.38)2.3
Total observations	64689	67026	64522	64971	81100	293430
Unique reflections	5410	5414	5421	5415	6567	12159
Completeness (%)[2]	99.1 (92.0)	99.1 (92.0)	99.1 (91.6)	99.0 (90.6)	98.9 (99.2)	98.3 (86.9)
Rmerge (%)[1, 2]	0.085 (0.263)	0.075 (0.264)	0.087 (0.298)	0.077 (0.308)	0.063 (0.410)	0.082 (0.428)
Redundancy[2]	12.5 (9.3)	12.4 (8.6)	11.9 (7.5)	12.0 (6.7)	12.3 (12.5)	24.1 (15.5)
I / σ<I>	13.2	12.9	11.8	12.2	16.4	15

[1] $Rmerge = \Sigma h \Sigma i \mid I(h)i - \langle I(h)\rangle \mid / \Sigma h \Sigma i \, I(h)i$,where $I(h)$ is the intensity of reflection h, Σh is the sum of all measured reflections and Σi is the sum of i measurements of reflection.

[2] Numbers in parentheses are the values for the highest resolution shell of each data set.

Table S2 Refinement statistics

Refinement Statistics		
Crystal	ADD_{3A}	H3-ADD_{3A}
Resolution range (Å)	28.8- (2.36)2.30	32.7- (2.35)2.29
Rwork (%)[1, 2]	20.9 (20.5)	19.2 (23.2)
Rfree (%)[1, 2]	25 (28.5)	22 (26)
R.M.S. deviations		
Bond length (Å)	0.012	0.013
Bond angle (°)	1.316	1.501
Ramachandran plot		
most favored (%)	89.4	94.5
additional arrowed (%)	10.6	5.5

[1] *R*work and *R*free = (Σ*hkl* ||*F*o| - |*F*c||) / Σ*hkl* |*F*o|, where the free reflections (5% of the total used) were held aside for *R*free throughout refinement.

[2] Numbers in parentheses are the values for the highest resolution shell of each data set.